EVLA Memo 216
A Search for Strong High-Frequency Low-Polarization Calibrators

Rick Perley

February 11, 2022

Abstract

The structures and polarizations of 40 VLA calibrator sources have been measured from 1 to 50 GHz with the VLA, while in its C configuration. The goal was to find sufficiently strong, unresolved and unpolarized sources suitable for polarization calibration of short-duration 'snapshot' observations. Of the 40, only four had sufficiently low polarization to serve as high-frequency polarization calibrators, and only one – J0319+4103 = 3C84 – is strong enough to provide sufficiently high SNR solutions at all bands. The dependence of the derived antenna solution accuracy on source fractional polarization and flux density is determined.

1 Introduction

Accurate astronomical polarimetry requires measurement and removal of the antennas' cross-polarization. For the VLA, the need for accurate measurement of the antenna cross-polarization leakages is particularly acute, as the wideband circular polarizers generally have high (5 – 10%) leakages.

There are two well-established methods available to measure the antenna cross-polarizations (often referred to as 'D' terms): – (1) Observe one or more calibrator sources through a large (typically 90 degrees or more) change in parallactic angle. The spread in parallactic angle permits measurement of the polarizations of the calibrators and the cross-polarizations of the antennas. (2) Observe a calibrator of known polarization.

The latter method has the advantage of requiring only a single observation – so is ideally suited for observations of short duration, but requires knowledge of the source polarization. The easiest application of this method occurs when the calibrator source has zero, or at least negligible, polarization. To my knowledge, neither of the two NRAO-supported calibration packages can make use of data from a polarized calibrator. But even if this capability is implemented, it would be of limited value, as both the flux density and polarizations from the flat-spectrum sources used for high frequency calibration are known to be variable, on timescales as short as weeks, or even days. The challenge of monitoring the flux densities and polarizations of the more than 1000 VLA calibrators, at all nine VLA bands, on a timescale short enough to track the variations in flux density and polarization, makes this unfeasable.

There are very few calibrator sources known to have zero, or close to zero polarization. Two CSS sources, OQ208 and J2355+4950, can be used at low frequencies, but both have steep spectra, and have insufficient flux density at high frequencies to enable their useage for polarization calibration. The only flat-spectrum source known to have negligible polarization, and enough flux density to be useful for high-frequency polarization calibration, is 3C84 = J0319+4130 – which although of moderately high declination, is below the reach of the array for about 10 hours a day. Clearly, a larger source list of unpolarized calibrators, suitable for high-frequency polarization calibration, is needed. If 3C84 is unpolarized from 1 to 50 GHz, we can hope there will be others.

To determine if there are such calibrators, I have used the time given to the Sept 2021 'flux density monitoring project' to determine the polarizations of 40 calibrator sources, mostly chosen for having high flux density at Q-band, and thus strong enough to be polarization calibrators, should their polarization fraction be low enough. It was known going into this project that the chance of finding one was not high – flat-spectrum objects are in general significantly polarized – typically 1 to 8 percent, and are variable, both in total flux density and in polarized flux and position angle. Despite these low odds, it was felt useful to try.

Answers to the questions of 'how strong must a calibrator be', and 'how low must the polarization be' for a calibrator to be useful for measurement of antenna polarization determination using the 'single observation method' are not well known. The data taken in this experiment gave answers to these important questions.

2 Source List and Observations

The source list was derived by selecting from the VLA Calibrator List the 24 sources, north of $\delta = -30$, with Q-band flux density greater than 3 Jy in 2002[1]. In addition to these, Lorant requested observations of three strong flat-spectrum sources near the galactic center. Also added were two known low-polarization CSS sources, the three northern flat-spectrum sources used to monitor system performance, and one other flat-spectrum source (J1130-1449) which was being used for referenced pointing for observations of Mars.

Eleven other sources – four planets, and seven standard flux density sources, were added for montitoring purposes, and to enable accurate flux density calibration. The final list – 44 sources – is given below.

- **Standard Flux Calibrators:** J0137+3309 = 3C48, J0437+2940 = 3C123, J0521+1638 = 3C138, J0542+4951 = 3C147, J0813+4813 = 3C196, J1331+3030 = 3C286, J1411+5212 = 3C295.
- **Northern Sources:** J0217+7349, J1153+8058, J1800+7828
- **Flat-Spectrum Sources:** J0238+1636, J0319+4130 = 3C84, J0359+5057, J0418+3801 = 3C111, J0501−0159, J0532+0732, J0607−0834, J0609−1542, J0730−1141, J0750+1231, J0927+3902, J1058+0133, J1229+0203=3C273, J1256−0547 = 3C279, J1337−1257, J1415+1320, J1549+0237, J1642+3948 = 3C345, J1733−1304, J1743−0350, J1751+0939, J1924−2914, J2148+0657, J2253+1608 = 3C454.3.
- **Known Low-Polarization Sources:** J1407+2827 = OQ208, J2355+4950
- **Planets:** Venus (1348−1203), Mars (1150+0156), Uranus (0249+1548), Neptune (2332−0417)
- **Others:** J1602+3326, J2225−0457 = 3C446, J2258−2758, J1130−1449

All objects were observed on Sept 09/10, 2021, at all the Cassegrain bands (L through Q), typically 3 to 5 times each, with each observation typical 15 seconds' duration. The details of the observations (time, frequencies, weather, calibration method) are fully described in EVLA Memo 214, and will not be repeated here. The array was in the 'C' configuration, resulting in a relatively low resolution of $\sim 20/\nu_G$ arcseconds, where ν_G is the observing frequency in GHz.

3 Data Selection and Imaging

After standard calibration of the 16 spectral windows provided at each frequency band, two spectral windows from each band (except, three at L-band), were selected for further processing – 17 spectral windows in all. These were chosen to be free from RFI, in order to simplify the imaging procedures. A basic self-calibration procedure was employed for each source. Images in I, Q, and U were produced for all sources, making a total of 2244 images (including the 204 planet images). For each, the integrated flux density and the 'nuclear' flux density for the three Stokes parameters (I, Q, U), were measured, along with the image rms. The determination of the 'nuclear' flux is somewhat subjective, as the resolution was often not sufficient to cleanly separate the nuclear flux from surrounding extended emission.

The frequencies selected for analysis, and the approximate resolutions of the images, are shown in the following table.

Table 1: **Frequencies and Resolutions in Arcseconds Utilized for the Imaging**

Band	Freq (MHz)	Res.	Band	Freq (MHz)	Res.	Band	Freq (MHz)	Res.
L	1011, 1424, 1808	13	X	8564, 10552	2.0	A	31936, 37064	0.6
S	2564, 3308	7	U	14192, 16820	1.3	Q	42064, 48064	0.4
C	4892, 7064	3.3	K	19442, 25435	0.9			

These data were imported into an Excel spreadsheet to enable determination of the fractional polarizations, position angles, and probable errors.

The resulting values for flux density fractional polarization, and polarization position angle, for both total and 'nuclear' components were then plotted as a function of frequency, spanning 1 to 50 GHz.

[1] That was the year the calibrator list was compiled. I thank Lorant Sjouwerman for extracting this information.

4 Results

4.1 Images

Most of the sources chosen for this program are not perfect point-source calibrators – there are usually some nearby, associated structures evident. In this section, I show example images of 24 sources, showing associated structures, selected at the band which shows the most structure. Sources which are not, or are partially resolved, are not shown. Of these sources, four (3C48, 3C138, 3C147, and 3C446) show partial resolution on sub-arcsecond scales, but the associated structures do not clearly appear in the contour images. The remaining 12 sources not shown here (J0217+7349, J1153+8058, J0238+1636, J0609−1542, J0730−1141, J1415+1320, J1743−0350, J1751+0939, J2148+0657, J1407+2827, J2355+4950, and J1602+3326) exhibit no structure to the limits of the resolution and sensitivity of these observations, nor any hint of nearby structure seen by examination of the visibilities. Higher resolutions will be required to find associated structures. In many cases, accurate measurement of these structures will be needed to make optimum use of them as calibrators.

In addition to nearby associated structures, all the observed fields show unassociated background objects. These rarely present any problem for calibration purposes for frequencies above typically 4 GHz, thanks to their normally steep spectra and the small primary beams at high frequencies. For lower frequencies, inclusion of these background objects into calibrator models becomes increasingly important.

'Postage-stamp' images of the 24 sources with identiable structures are shown in the following six figures. The detectable polarizations are superposed as dashes, with the dash length proportional to the fractional polarization, and the orientation that of the observed E-field. No attempt was made to correct for Faraday rotation. Comments on individual sources are provided. Note that these images result from a total of 60 seconds integration, in 3 to 5 snapshot observations.

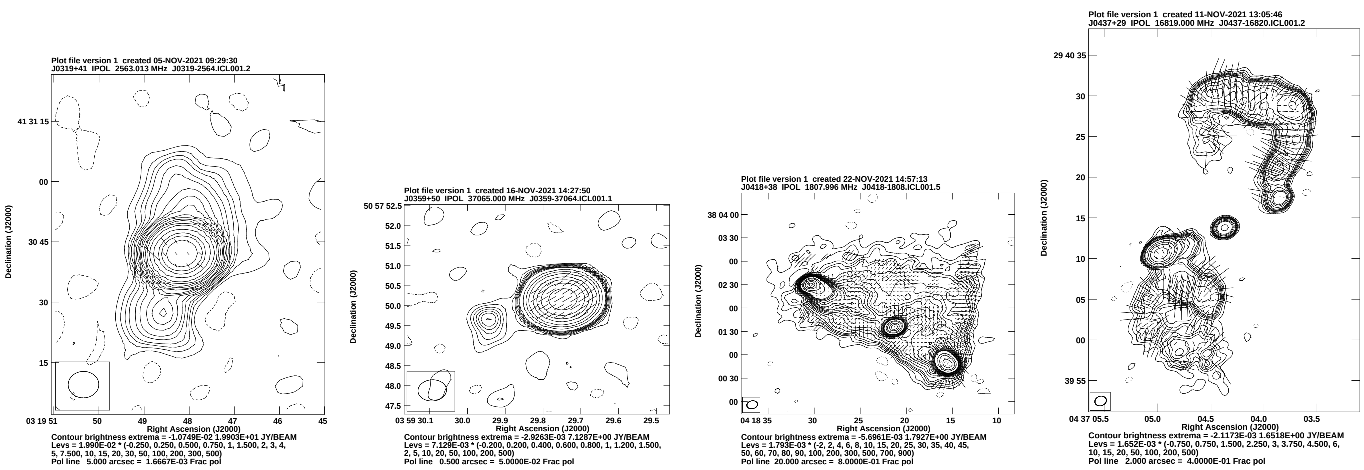

Figure 1: Maps of 3C84 at 2564 MHz, J0359+5057 at 37 GHz, 3C111 at 1808 MHz, and 3C123 at 16.8 GHz.

Fig 1 3C84 (left panel) has a very extended low-frequency halo of near 10 arcminutes extent, not visible in this image, but clearly evident in the L-band images. With higher resolution, the nuclear core is also found to be resolved into small extensions of tens of milliarcseconds extent, along the same N-S axis as the 'ears' seen in this image. 3C111 (middle right panel) is an unusual combination of a very bright nucleus, bright and compact hotspots, and highly polarized, extended emission which uniformly fills the regions spanned by the bright structures. A highly collimated jet, extending towards the NE hotspot, is clearly seen in the higher resolution images. The extended structures are undersampled at higher frequencies, so the total flux of the source is quite uncertain. The extended structure of 3C123 (right panel) is well represented in this image. At the highest frequencies, all the extended structures are resolved out, but the nucleus, at ∼80 mJy, is too weak to serve as a useful calibrator.

Fig 2 None of the four sources shown in the plot have any associated associated structures other than what is visible.

Fig 3 3C196 (left panel) contains a very weak nucleus, of less than 2 mJy. None of the four sources shown in this figure contain any other associated detectable structures.

Fig 4 The jet shown in 3C273 (left panel) is the only detectable structure outside the nucleus. The flux

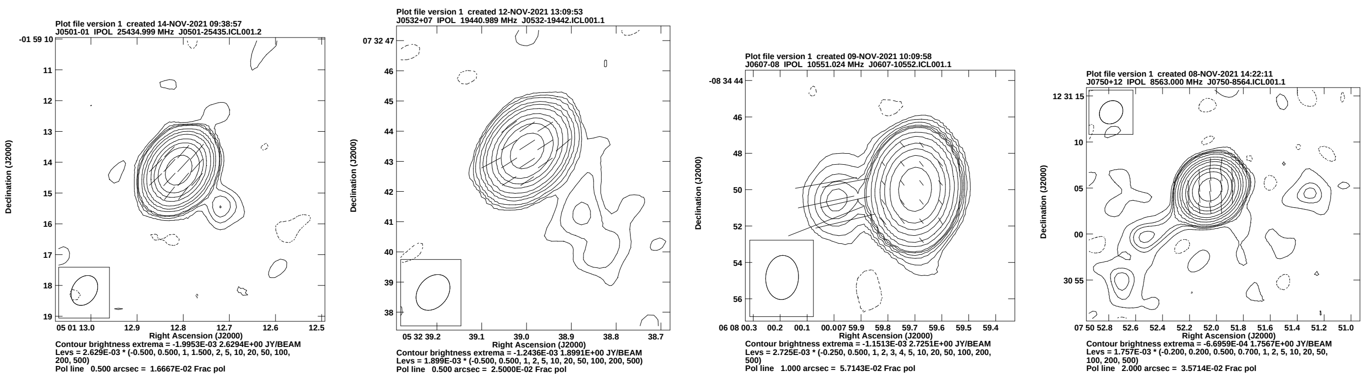

Figure 2: Maps of J0501−0159 at 25.4 GHz, J0532+0732 at 19.4 GHz, J0607−0834 at 10.6 GHz, and J0750+1231 at 8.6 GHz.

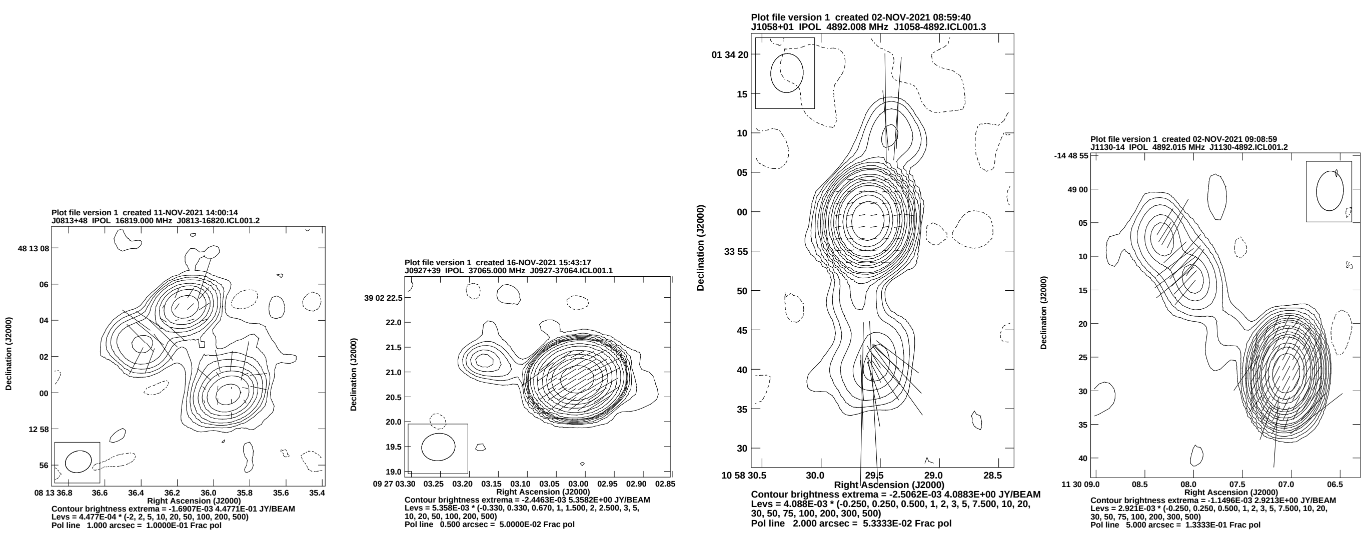

Figure 3: Maps of 3C196 at 16.8 GHz, J0927+3902 at 37.1 GHz, J1058+0133 at 4.9 GHz, and J1130−1449 at 4.9 GHz.

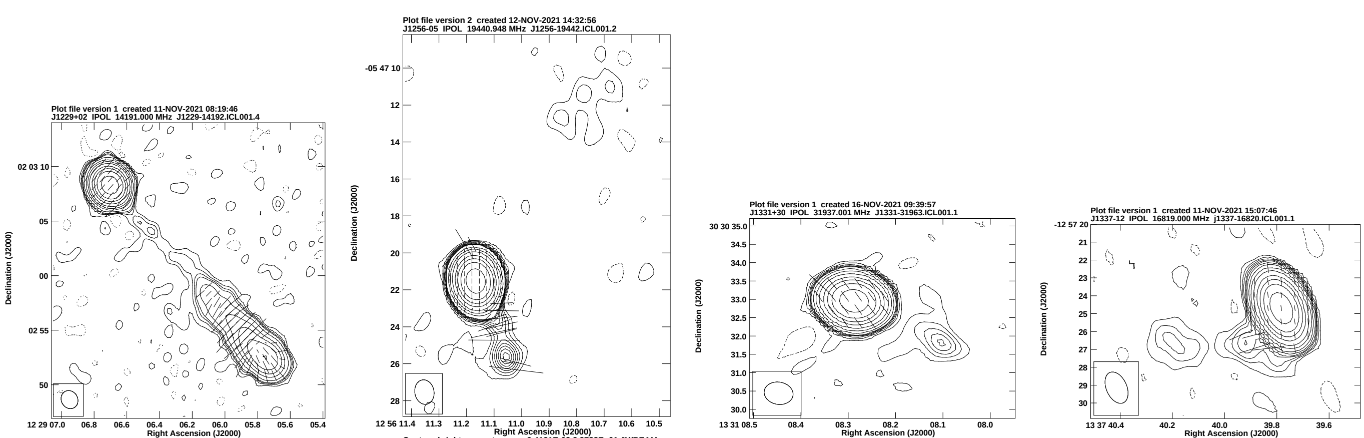

Figure 4: Maps of 3C273 at 14.2 GHz, 3C279 at 19.4 GHz, and 3C286 at 32 GHz and J1337−1257 at 16.8 GHz.

and fractional polarization of the nucleus have changed significantly in the past few years. The weak extended emission seen in 3C279 (center left panel) no the NW of the nucleus has a very steep spectrum, and is quite bright at the lower frequencies. 3C286 (center-right panel) comprises another small component, visible in A-configuration images, located 1 arcsecond to the east of the nucleus, and another one 0.4 arcseconds to the SW. J1337−1257 (right panel) shows no detectable structures other than that shown here.

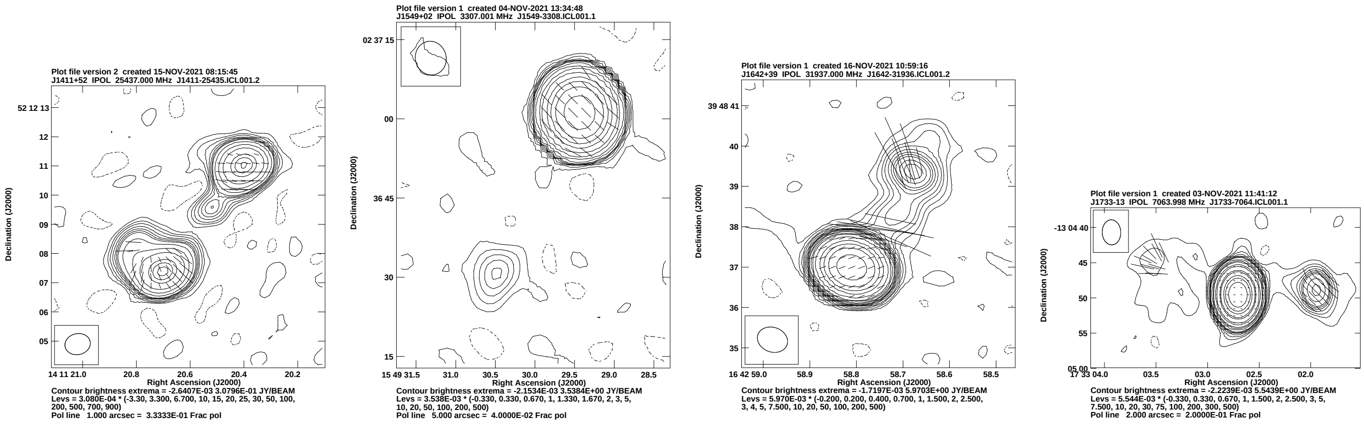

Figure 5: Maps of 3C295 at 25.4 GHz, J1549+0237 at 3.3 GHz, 3C345 at 31.9 GHz, and J1733−1304 at 7.1 GHz.

Fig 5 3C295 (left panel) contains a weak nucleus, of ∼8 mJy, far too weak to be useful as a calibrator. The source shows no detectable structure beyond what is shown, at any band. J1549+0237 (center left panel) shows no structures beyond what are seen in the image. 3C345 (center right panel) has quite complex additional structure – extending ∼17 arcseconds to the north and south, evident in the low frequency images, but resolved out above 15 GHz. There are no other detected structures visible beyond what is shown for J1733−1304 (right panel).

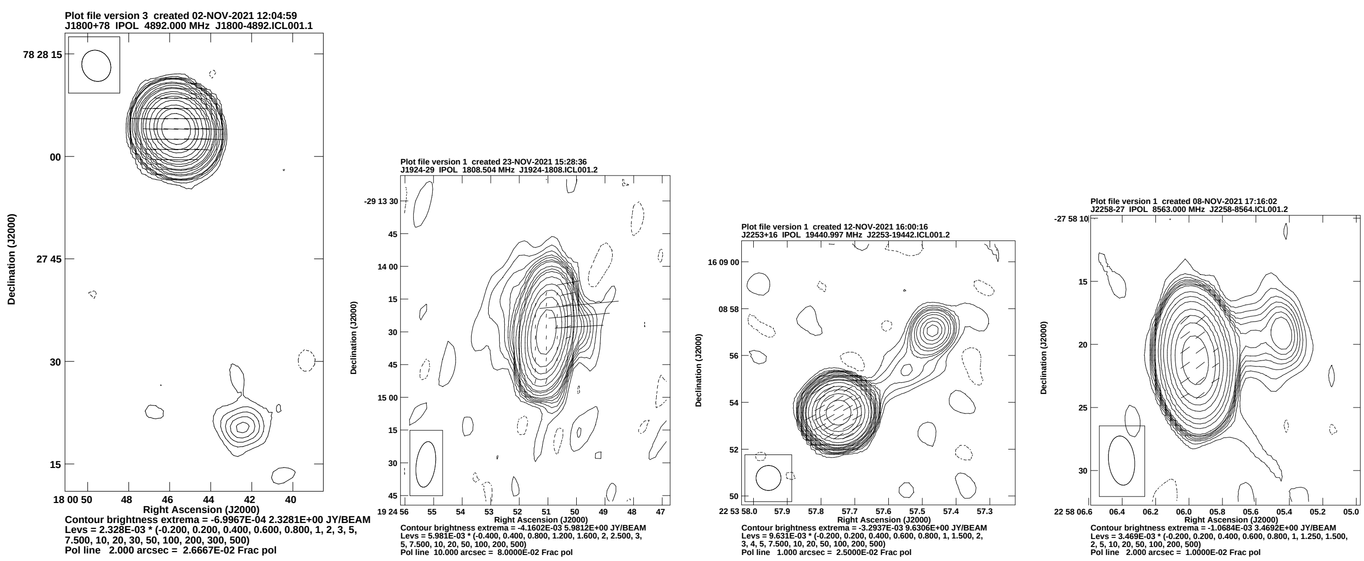

Figure 6: Maps of J1800+7828 at 4.9 GHz, J1924−2914 at 1.8 GHz, 3C454.3 at 19.4 GHz, and J2258−2758 at 8.6 GHz.

Fig 6 The weak associated structures in J1924−2914 (center-right panel) are not seen above 5 GHz, and there are no other visible associated structures. There are no other detected structures visible at any band, beyond what is shown, for the remaining sources in this figure.

4.2 Polarization

The polarization data for 38 of the 40 calibrator sources are shown in Figs 7 through 19. The sources not shown (3C196, and 3C295) have both complicated polarization structures associated with their lobes, and very weak nuclei – a combination which makes them unsuitable as a polarization calibrator at any band or resolution of the VLA.

The three panels for each source show the flux density (top), percentage linear polarization (middle), and linear polarization position angle (bottom). The black traces show the nuclear component values, the red traces the total, integrated values. All quantities are ploted against the logarithm of frequency from 1 to 50 GHz.

The position angle plots commonly show discontinuities at the lower frequencies – commonly below 3 GHz. This is due to a modest rotation measure (RM) rotating the plane of polarization by more than one-half turn between adjacent frequencies. For some sources, I have 'unwrapped' the ambiguity, to show the true position angle. But in others, with higher RMs, this has not been done in order to keep the position angle span (y-axis) small enough that the details of the high frequency data are retained. In all cases, a continuous rotation of the plane of polarization as the frequency decreases can be found.

Although errors in the images were measured for all sources, I have elected to not add the estimated error bars in the following plots. For all bands except Q-band, and all sources except those with polarization less than 1%, these formal errors are less than 0.1% in polarization, and 1 degree in phase. The apparent 'zig-zag' polarizations above 40 GHz for some of the weaker sources shown in these plots are due to random errors.

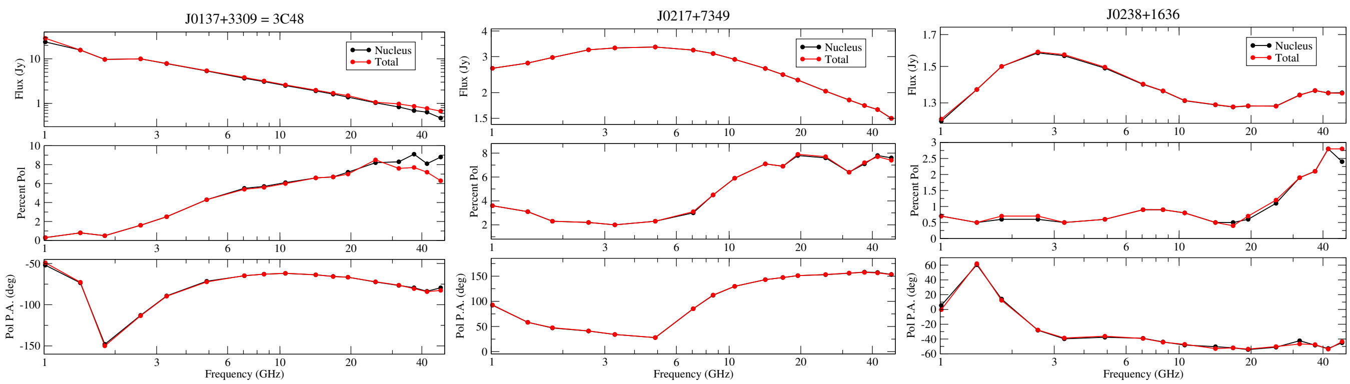

Figure 7: Polarization data for 3C48, J0217+7349, and J0238+1636. The separation between nucleus and total for 3C48 is real, as the small-scale extended structure is clearly resolved above 35 GHz.

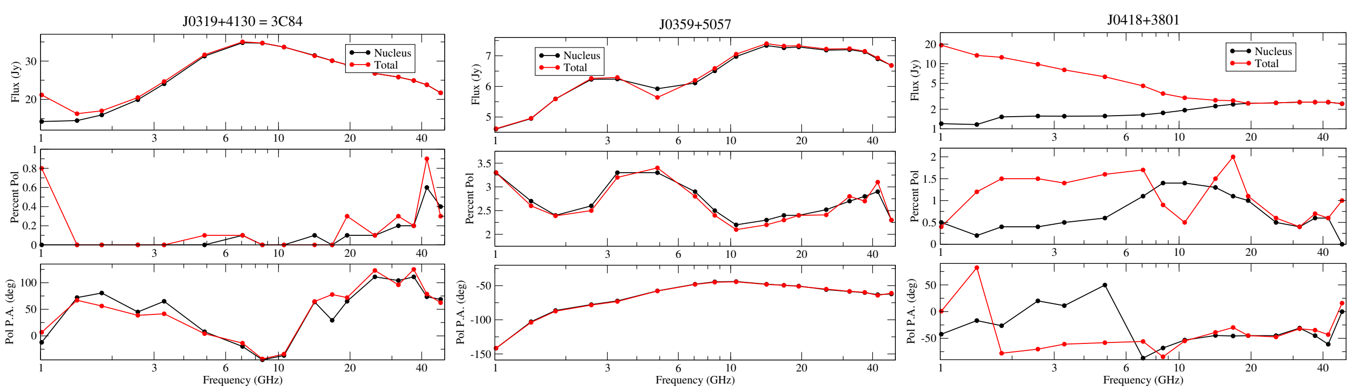

Figure 8: Polarization data for 3C84, J0359+5057 and 3C111. The last of these includes very extended structure at the lower frequencies, so the 'total' fluxes and polarizations are very uncertain. The values shown for 3C84 are all upper limits, except possibly at Q-band.

The complex fractional polarization and position angle data shown in these plots provides strong evidence for multiple (unresolved) components and/or multiple magnetoionic screens. For example, the polarized emission below 8 GHz for 3C454.3 (seen in the right panel of Fig 18) shows the likely presence of a Faraday rotating screen witn RM ~ 47 rad/m^2. However, the higher freqeuency emission shows the presence of another polarized component, which is either rotated by a much higher RM (~ -1450 rad/m^2), or which has a changing position angle with increasing frequency, possibly due to a spectral index gradient down the relevant component. The complex combination of these two components is responsible for the minimum in fractional polarization seen near 10 GHz – at that frequency, the two components' polarized flux are equal and orthogonal.

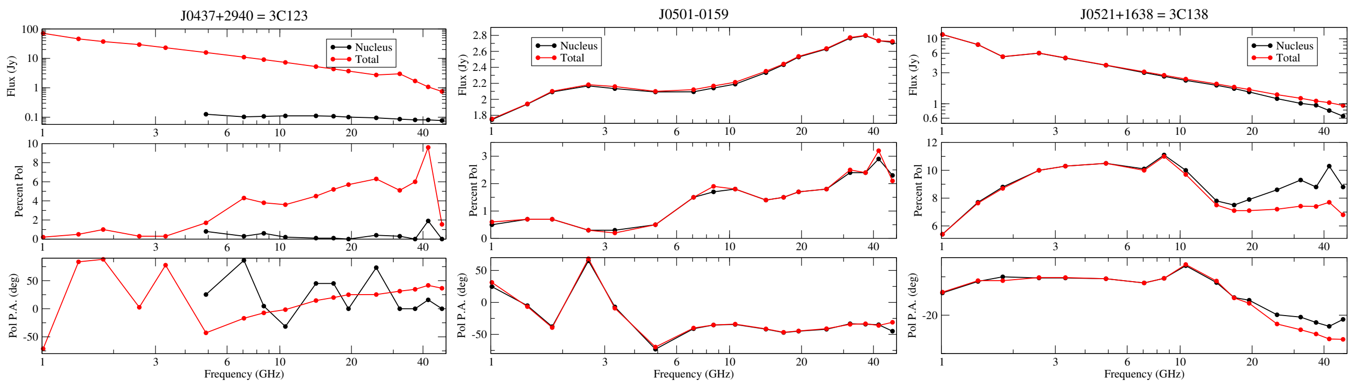

Figure 9: Polarization data for 3C123, J0501−0159 and 3C138. The highly polarized nuceus and jet in 3C138 are separable above 20 GHz.

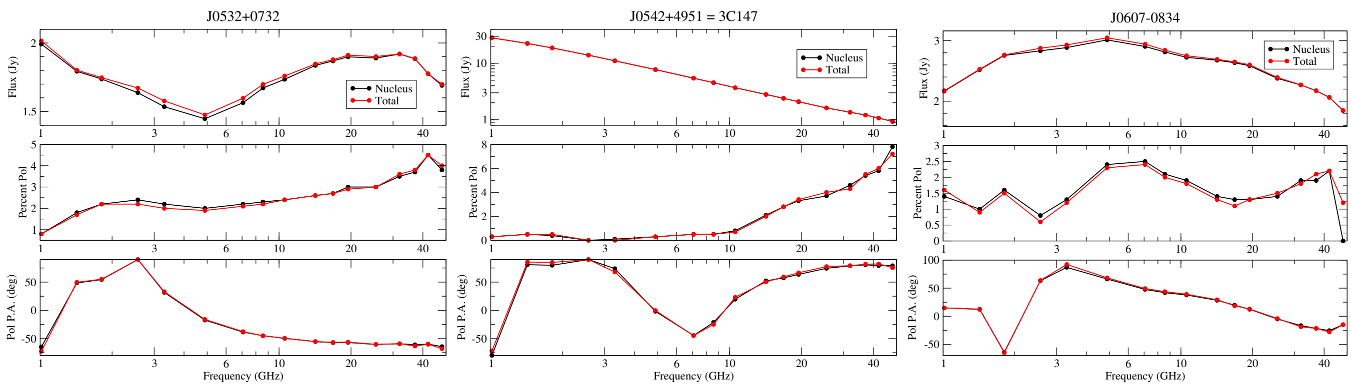

Figure 10: Polarization data for J0532+0732, 3C147, and J0607−0834.

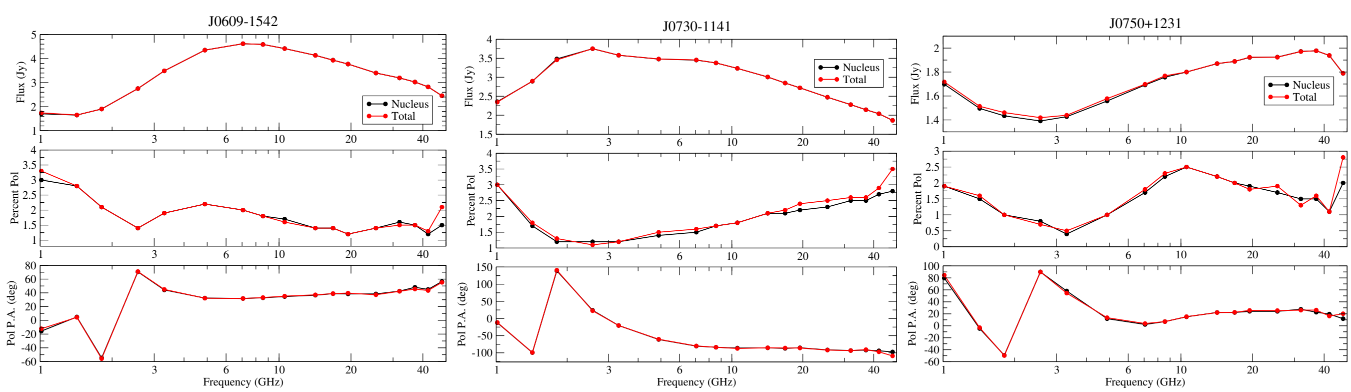

Figure 11: Polarization data for J0609−1542, J0730−1141, and J0750+1231.

5 Polarization Accuracy vs. Source Strength and Polarization Fraction

I noted in the introduction that there are two established methods for measuring the antenna cross-polarization – one involving tracking one or more strong calibrators over a wide range in parallactic angle, the other requiring one or more observations of a strong, unpolarized source[2]. The latter method is very convenient, as it requires only one observation, and is indeed the only viable method for the increasingly common observational mode of short duration scheduling blocks.

But – how unpolarized must a source be for this method to work? Is 0.5% low enough? 1%? Similarly –

[2]Use of a source of known polarization should be possible, but is not implemented in software at this time.

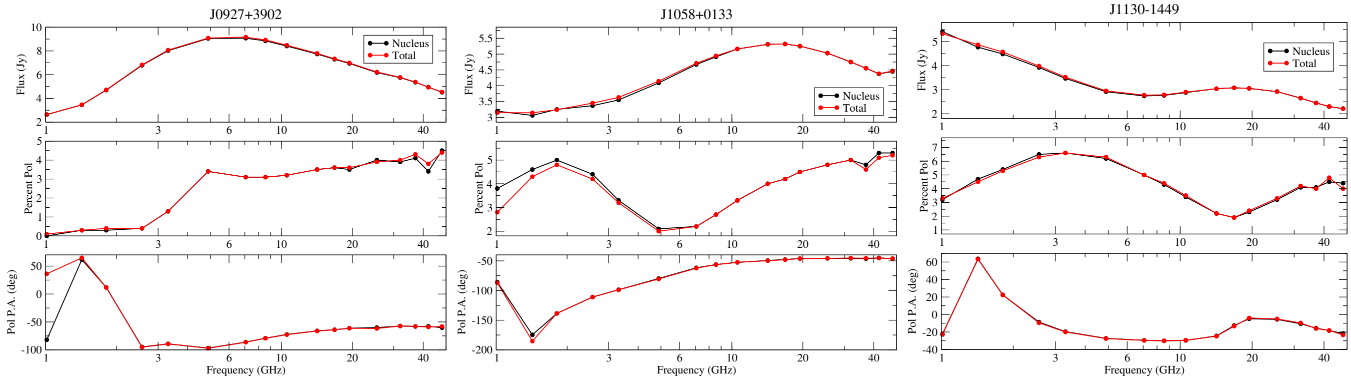

Figure 12: Polarization data for J0927+3902, J1058+0133, and J1130−1449.

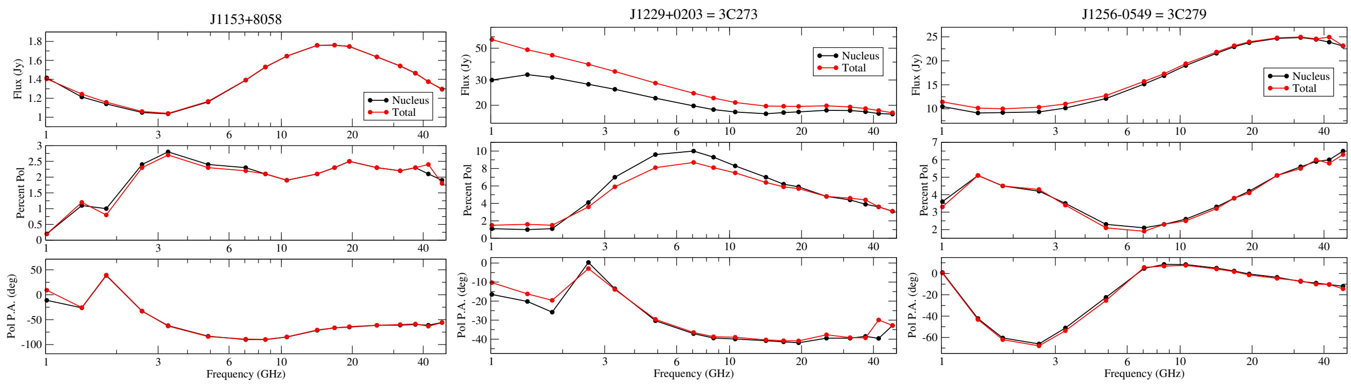

Figure 13: Polarization data for J1153+8058, 3C273, and 3C279.

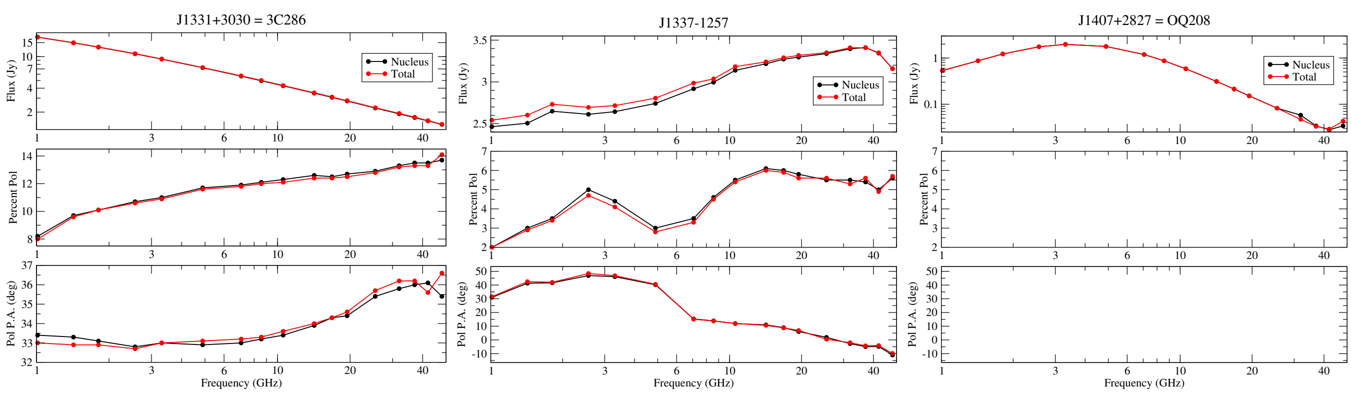

Figure 14: Polarization data for 3C286, J1337−1257, and J1407+2827 = OQ208. The last of these is completely unpolarized and unresolved over the entire frequency range, but is too weak to serve as a polarization calibrator at high frequencies.

how strong must the source be? Will a 1 Jy unpolarized source suffice? Finally – what duration should the scan have to provide an acceptable result?

Although these questions can be answered by relatively straightforward analysis, the data taken in the 2021 Flux Densities Run provides the data needed to directly answer these questions. The 'gold standard' solution is provided by the standard method of determining the cross-polarizations – using the data from 30 unresolved sources observed over the entire 24-hour observation. For the 'single snapshot' method, I used various calibrators of varying strengths and fractional polarizations.

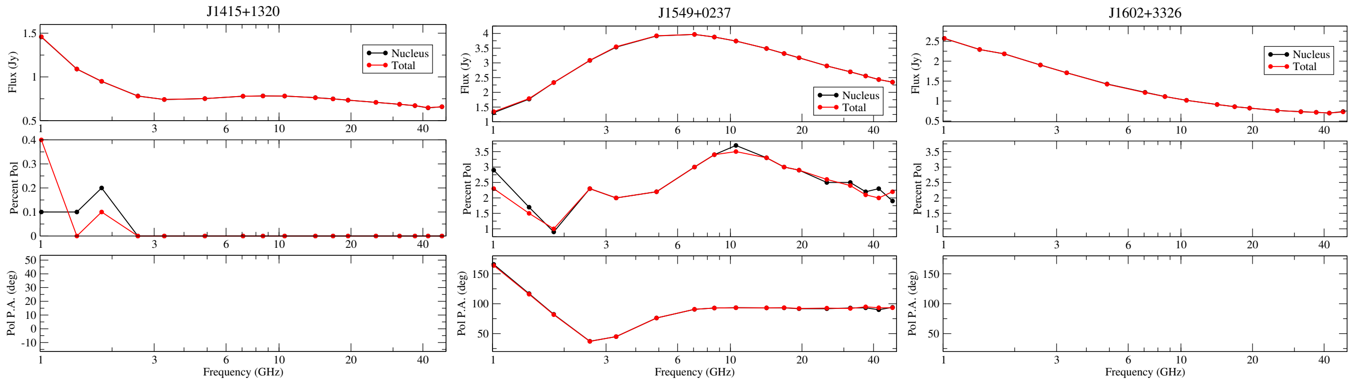

Figure 15: Polarization data for J1415+1320, J1549+0237, and J1602+3326. The last of these has not detectable polarization at any band, but is too weak to serve as a 'snap-shot' polarization calibrator at high frequencies.

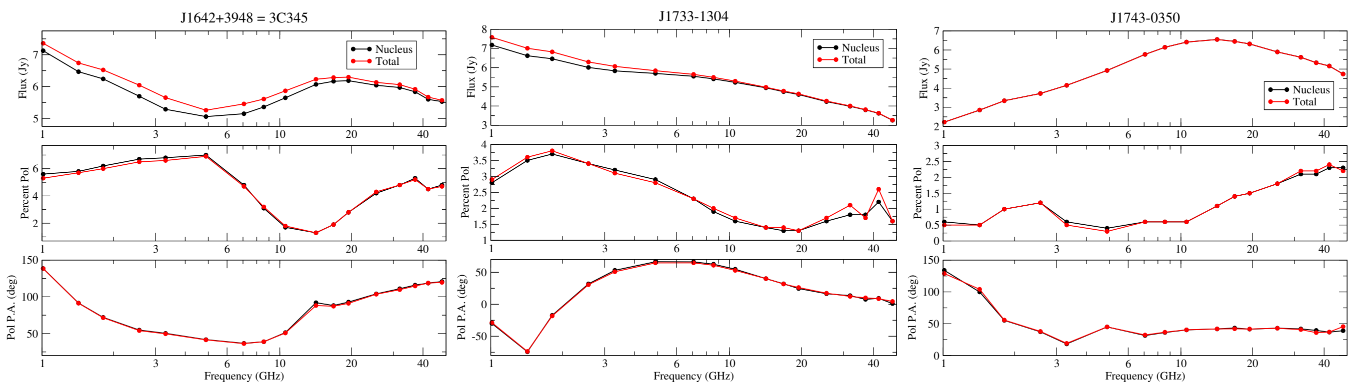

Figure 16: Polarization data for 3C345, J1733−1304, and J1743−0350.

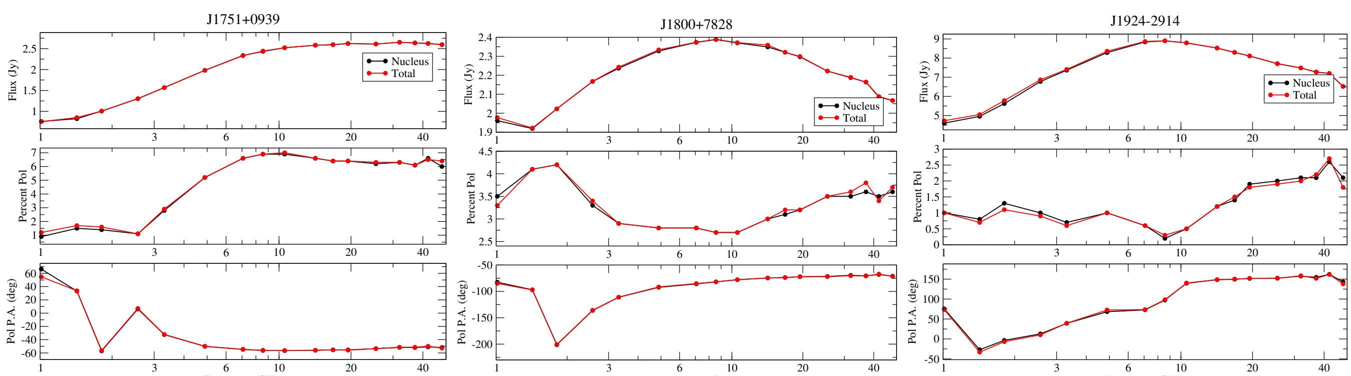

Figure 17: Polarization data for J1751+0939, J1800+7828, and J1924−2914.

5.1 Test 1: Comparison of the two methods

Here I compare the 'standard' solution to that provided from a single, very strong, unpolarized source. For this, I chose 3C84, which at Ku-band has a flux density of 30 Jy, and is less than 0.1% polarized, and at Q-band has 24 Jy flux density and is marginally polarized ($\sim$ 0.6%). The software finds the cross-hand leakages assuming zero source polarization. For this determination, ea11 was taken as the 'reference' antenna, meaning that the software assumes that 11R is 'pure' – *i.e.* that there is no coupling of signals between 11L to 11R. The 'D' terms for ea07 – a very typical antenna – for both methods are shown in Fig 20. The D terms are defined in terms of voltages, and are normalized by the source total flux density. As seen in the figure, there is no discernible difference between these solutions. The conclusion is that the two methods – with sufficient SNR, and parallactic angle coverage – give the same solutions. The high 'bump' in RCP to LCP cross-polarization seen in SPW 6

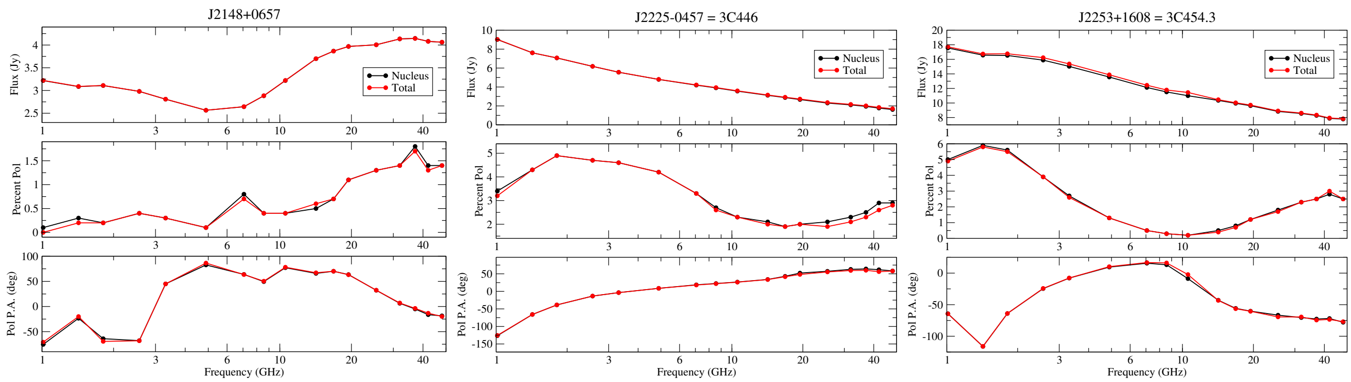

Figure 18: Polarization data for J2148+0657, J2225−0457 = 3C446, and J2253+1608 = 3C454.3. The visibilities for 3C446 indicate a large, extended halo surrounding the compact nucleus. The presence of complex structure is also suggested by the polarization data.

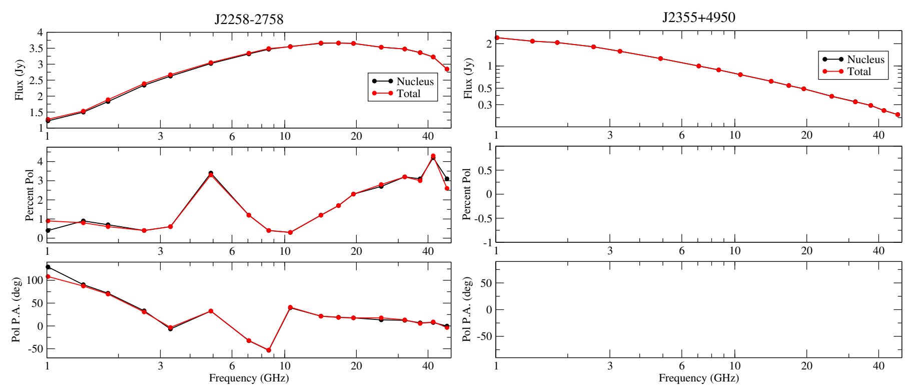

Figure 19: Polarization data for J2258+2758 and J2355+4950. The latter source is completely unpolarized and unresolved, but is too weak at high frequencies to serve as a 'snapshot' polarization calibrator at high frequencies. .

at Ku-band is seen in all antenna solutions, except the reference antenna ea11, which strongly implies that it originates in the reference antenna.

5.2 Test 2: Dependence on Fractional Polarization

This test answers the question: How low a fractional polarization is needed to return a reliable solution. To answer this, I determined the cross-polarizations of ea04 at 19 GHz (K-band), using four strong sources with increasing polarizations: (1) 3C84 (29 Jy, 0.1% polarization), (2) J1743-0350 (6.3 Jy, 1.5% polarization), (3) J0359+5057 (7.3 Jy, 2.4% polarization), and (4) J0927+3902 (6.9 Jy, 3.5% polarization). The results are shown in the left panel of Fig 21. The red, gold, green, and blue traces correspond to the four sources listed above. It is significant that the LCP to RCP leakages (top panel) are nearly the same for all four sources, while the RCP to LCP leakages, shown in the lower panel, show an increasing deviation from the correct values as the fractional polarization rises. These increases are by approximately that of the fractional polarized flux. This difference in behavior between the L to R leakage, and the R to L leakage, is seen in all antennas. Evidently, the source fractional polarization has been transferred to the RCP to LCP solution of the reference antenna, and from there to the RCP to LCP solutions for all others. The conclusion here is that a polarization of less than 1% is needed to generate a solution accurate to that level.

5.3 Test 3: Strength of the Calibrator

.

Here I used four sources of low polarization (<1%) of varying flux densities: (1) 3C84 (29 Jy, < 0.1%), (2) J2146+0657 (4.0 Jy, 1.0%), J0238+1636 (1.3 Jy, 0.6%), and J2355+4950 (0.70 Jy, <0.7%) at K band (18.7 –

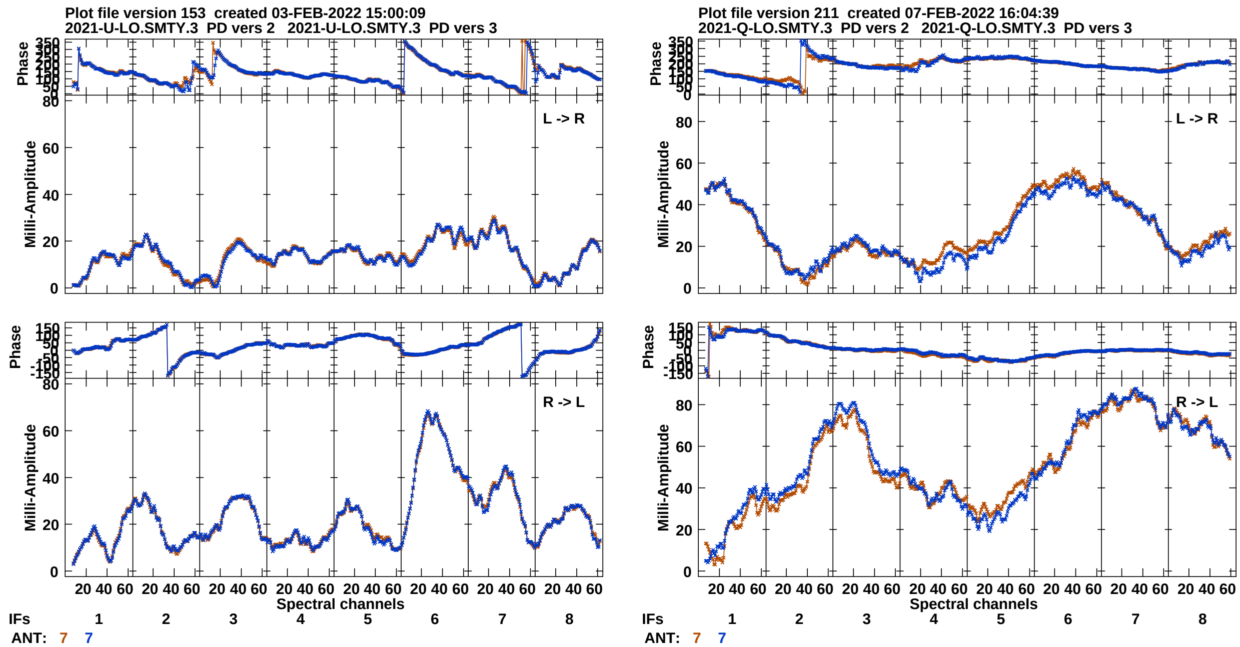

Figure 20: Comparison of the cross-polarization solutions, relative to 11R, for ea07 at Ku-band (left, 13.6 – 14.5 GHz) and Q-band (right, 41.5 – 42.4 GHz). Upper panels: Leakage from LCP to RCP, phase above and amplitude below. Lower panels: Leakage from RCP into LCP. The red tracks show the solutions using 30 unresolved sources and all 24 hours' data, (total on-source time about 30 minutes, and an average flux density of about 5 Jy) while the blue trace is that from five observations of 3C84, each of 15 seconds duration. The solutions are indistinguishable at Ku-band, and are only slightly different at Q-band, likely due to the small polarization of 3C84 at that band.

19.7 GHz). The resulting D-term solutions are shown in the right-hand panel of Fig 21. These are colored red, gold, green, and blue, in order of decreasing flux density.

The figure shows that all four sources give unbiased solutions, but the scatter seen in these plots for the two weaker sources show that a flux density more than 2 Jy is needed to give solutions more accurate than the fluctuations seen in the actual cross-polarization on frequency scales less than the SPW width (128 MHz).

5.4 Analysis and Discussion

The cross-polarizations shown in the figures above are typical for the EVLA polarizers at all bands – the values are uncomfortably high (often higher than 5%), and have considerable frequency structures on scale much less than the SPW width (typically 128 MHz). This latter point means that a relative fine frequency resolution (certainly finer than 10 MHz, if resonance effects such as that seen in Fig 21 are to be accounted for) is required for accurate removal of the cross-polarization leakages.

The left panel of Fig 21 shows how the increasing fractional polarization of the (assumed unpolarized) calibrator sources couples into the derived cross-polarizations. The surprise (for the author) is that the top panel (LCP to RCP coupling) is relative immune to source polarization, while the opposite leakage (bottom panel) is highly sensitive to the source polarization. All antennas show this, and the origin is easy to find – it is due to the cross-polarization solution of the reference antenna (ea11 in this case). Evidently, the true fractional polarization of the source is being interpreted as an antenna polarization, in addition to the relative cross-polarization of the antenna itself. The offset in the antenna polarization solution due to the source polarization is roughly equal to the fractional polarization of the source. Thus, if we believe we need a 1% accuracy in the determination of the 'D' terms, then we must use a source with less than 1% fractional polarization.

The right panel shows the growth in the solution noise as the strength of the source decreases. For this antenna and band, the peak-to-peak errors in the solution are roughly 4% for the weakest source (flux 0.7 Jy). Examination of this and other plots shows that the solution noise is inversely proportional to the calibrator flux density, as expected.

Simple sensitivity arguments suggest that the solution noise will scale with the array SEFD , and inversely

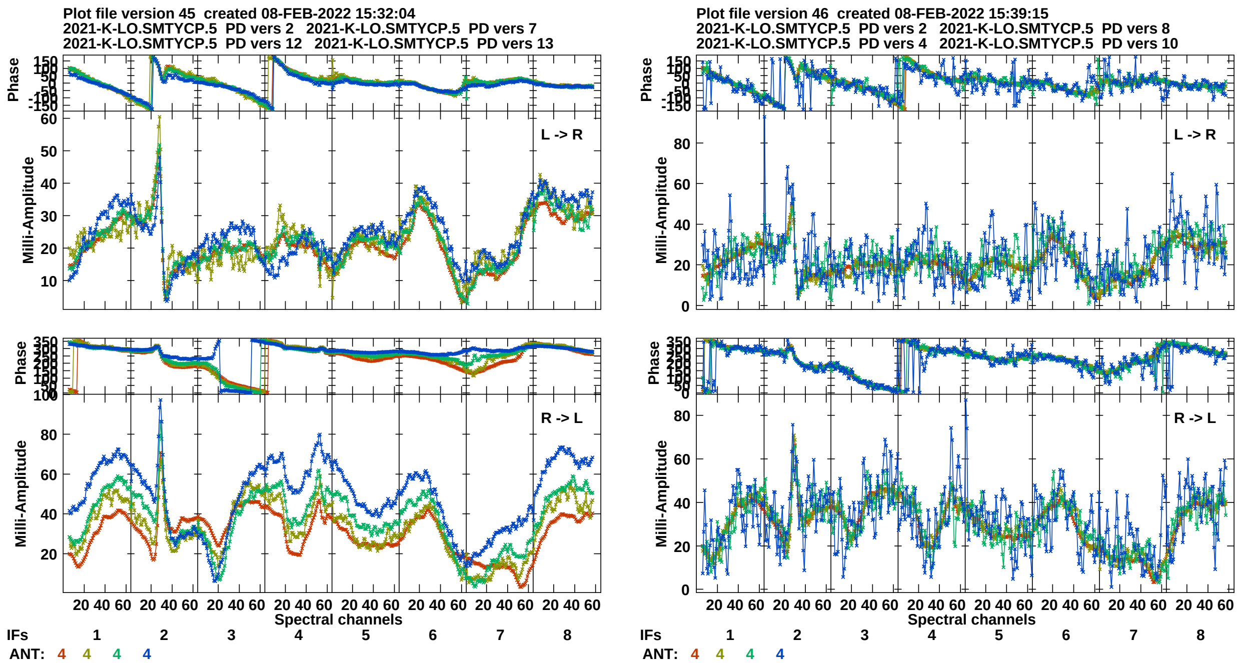

Figure 21: (Left) Showing the cross-polarization solutions for ea04, using four strong sources of increasing fractional polarization, at K-band (18.7 – 19.7 GHz). The red trace shows 3C84, equal to the multiple-source values. The gold, green, and blue traces show increasing deviations in the solutions from the correct (relative) values as the fraction polarization of the calibrator source increases. (Right) Showing increase in solution noise with decreasing flux density, for the same antenna and frequencies as the left panel. The four sources used here are all negligibly polarized.

with the number of antennas, calibrator source flux and the square root of the bandwidth-time product. The proportionality factor can be derived from the current observations. Using the values given above, and the known SEFD for Ku-band (450 Jy), we drive the following rough relationship between the pk-pk errors in the polarization determination (in percent) to source flux and system paramters:

$$\sigma_{\%} \sim \frac{2SEFD}{N_{ant} S_{Jy} \sqrt{\Delta\nu_{MHz} \Delta T_{sec}}} \tag{1}$$

At Q-band, the SEFD > 1000 Jy, which suggests that a 10Jy unpolarized calibrator is required for 1% maximum solution error, if the standard correlation resolution (2 MHz), and 1 minute observation, is desired. Decreasing spectral resolution, and spending more time on the source will reduce the errors, but a factor of 25 increase in the Bandwdith-Time product is needed to reduce the maximum errors to 1% for a $\sqrt{25} = 5-$fold reduction in the calibrator flux density – *i.e.* a 2 Jy calibrator.

The same analysis will apply to the ‘traditional’ polarization calibration method. Here, the time T will correspond to the total time spend on the calibrator(s) used in the observation.

6 Summary

Observations of the two dozen strongest Q-band calibrators has found only one source both strong enough and unpolarized enough to serve as an antenna cross-polarization calibrator suitable for short duration high frequency observations. That source is 3C84, already well known as a suitable source. Three other sources: J1407+2827 = OQ208, J1602+3326, and J2355+4950 are all unpolarized over the full 1−50 GHz range of the VLA, but all have steep spectra, with less than 1Jy flux density above 10 GHz, making them of little use for polarization calibration at high frequencies.

Test solutions using the ‘zero-polarization’ single-source method show that the accuracy of the derived antenna polarization is limited by the fractional polarization of the calibrator. If the calibrator’s true polarization is x%, the resulting D-term solutions will be in error by roughly this amount. The SNR of the derived cross-polarization solutions scales as expected the calibrator source flux. An approximation of the relation is derived, from which the bandwidth-time product needed to determine a solution with the desired accuracy can be determined for a given calibrator flux density.

7 Acknowledgements

Many thanks to Eric Greisen for his efforts in modifying AIPS tasks to permit better analysis and presentation of these results, and to Lorant Sjouwerman, for a careful read and useful feedback.